JCTC Journal of Chemical Theory and Computation

Article

pubs.acs.org/JCTC

Accurate Computation of Cohesive Energies for Small to Medium-Sized Gold Clusters

Bun Chan*,† and Wai-Leung Yim*,‡

†School of Chemistry and ARC Centre of Excellence for Free Radical Chemistry and Biotechnology, University of Sydney, NSW 2006, Australia

‡Institute of High Performance Computing, Agency for Science, Technology and Research, 1 Fusionopolis Way, No. 16−16 Connexis, Singapore 138632

Supporting Information

ABSTRACT: High-level CCSD(T)-F12-type procedures have been used to assess the performance of a variety of computationally less demanding methods for the calculation of cohesive energies for small to medium-sized gold clusters. For geometry optimization for small gold clusters, the PBE-PBE/cc-pVDZ-PP procedure gives structures that are in close agreement with the benchmark geometries. We have devised a CCSD(T)-F12b-based composite protocol for the accurate calculation of cohesive energies for medium-sized gold clusters. Using these benchmark (nonspin−orbit vibrationless) cohesive energies, we find that fairly good agreement is achieved by the PBE-PBE-D3/cc-pVTZ-PP method. In conjunction with PBE-PBE/cc-pVDZ-PP zero-point vibrational energies and spin-obit corrections obtained with the PBE-PBE-2c/dhf-TZVP-2c method, we have calculated 0 K cohesive energies for Au_2−Au_{20}. Extrapolation of these cohesive energies to bulk yields an estimated value of 383.2 kJ mol^{-1}, which compares reasonably well with the experimental value of 368 kJ mol^{-1}.

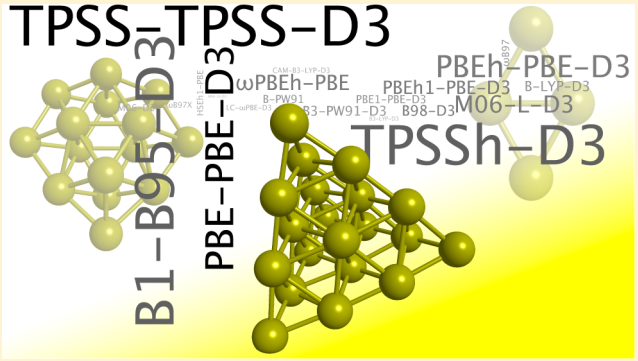

INTRODUCTION

Gold clusters and nanoparticles have attracted considerable attention in recent years, owing in part to their potential applications in a range of areas.[1] Many studies on these species were carried out using computational quantum chemistry, typically with density functional theory (DFT) procedures.[2] There have also been a number of theoretical investigations using high-level wave-function-type methods such as CCSD-(T).[3]

The two categories of theoretical procedures, namely DFT and high-level wave-function-type methods, both have their strengths and disadvantages. While DFT has a reasonably low demand on computational resources and can be applied to relatively large gold clusters, it can sometimes give quite inaccurate results. On the other hand, high-level wave-function-type procedures are in general accurate but can be very demanding on computational resources and are therefore applicable to only small clusters. Thus, in order to advance the theoretical study of gold clusters of medium to large sizes, it is of critical importance to evaluate the performance of DFT procedures, and it is advantageous to devise computationally less demanding but still accurate wave-function-type protocols for these systems.

In the present study, we attempt to provide advancements in both aspects. We evaluate the performance of a variety of computational chemistry procedures for the calculation of cohesive energies (CEs, atomization energies per atom) for gold clusters of increasing size:

$$\mathrm{CE}(\mathrm{Au}_n) = 1/n \times [nE(\mathrm{Au}) - E(\mathrm{Au}_n)] \quad (n = 2\text{−}20)$$

We first assess the performance for small gold clusters for high-level wave-function-type procedures that are of reduced demand on computational resources. We then use the optimal high-level method to additionally obtain accurate benchmark energies for medium-sized gold clusters for the evaluation of DFT procedures.

COMPUTATIONAL DETAILS

Standard ab initio molecular orbital theory and DFT calculations[4] were carried out with the Gaussian 09,[5] Molpro 2010,[6] and Turbomole 6.4[7] programs. For geometry optimizations, we have examined a number of DFT methods as well as high-level CCSD(T)-type procedures. Gold clusters can adopt a number of conformations. For Au_2−Au_8, the conformational spaces have been previously examined with high-level CCSD(T)-type procedures.[3b,c,e] In the present study, we have adopted the lowest-energy conformers found in these studies as our initial structures. The conformers of larger gold clusters (as large as Au_{20}) have been examined with several

Received: January 19, 2013
Published: March 25, 2013

ACS Publications © 2013 American Chemical Society

DFT procedures.[8] For these clusters, namely Au_9−Au_{20}, we have examined all low-energy conformers presented in ref 8.

Following each geometry optimization, harmonic frequency analysis was carried out to confirm the nature of the stationary point as an equilibrium structure. To obtain the zero-point vibrational energies (ZPVEs), we used unscaled harmonic vibrational frequencies. Our benchmark energies were calculated using the CCSD(T)-F12a procedure[9] or protocols that employ the related CCSD(T)-F12b method[9] as key ingredients. These F12-type methods include explicit two-electron terms to enable more rapid basis set convergence than conventional (one-electron) procedures, thus allowing the use of smaller and computationally less demanding basis sets while maintaining a similar accuracy.[10] The F12a and F12b variants are approximations to the full F12 method. They include different subsets of two-electron terms found in full F12.[9]

A number of basis sets were employed in the present study. These include Ahlrichs-type basis sets def2-SVP, def2-TZVP, and def2-QZVP[11] and Dunning-type basis sets cc-pVDZ-PP, cc-pVTZ-PP, and cc-pVQZ-PP.[12] In all calculations, the 60 inner-shell electrons were treated using effective core potentials (ECPs) that are complementary to the basis sets employed.[13] This approach not only substantially reduces the computational demand but also implicitly includes scalar-relativistic effects into the calculations. The contributions of spin−orbit effects to the adhesive energies (ΔE_{SO}) were evaluated using two approaches. Thus, we have calculated ΔE_{SO} using the two-component treatment[14] as implemented in Turbomole at the PBE-PBE[15] level (i.e., PBE-PBE-2c) in conjunction with the dhf-TZVP-2c basis set.[16] We have also estimated these values using the empirical formula[3d] $\Delta E_{SO} = 3.0 \times N_{atom} + 9.5 \times N_{bond}$, where N_{atom} is the number of gold atoms and N_{bond} is the number of formal bonds in a particular cluster. All interatomic distances are given in Å, and relative energies are presented in kJ mol^{-1}.

We have examined a number of prototypical DFT procedures in the present study. These include the pure functionals B-LYP,[17] B-PW91,[18] PBE-PBE,[15] PBEh-PBE,[19] ωPBEh-PBE,[20] TPSS-TPSS,[21] and M06-L[22] and the hybrid DFT procedures B3-LYP,[23] B3-PW91,[24] CAM-B3-LYP,[25] PBE1-PBE,[26] PBEh1-PBE,[15] LC-ωPBE,[27] HSEh1-PBE,[20] TPSSh,[21] B1-B95,[28] B98,[29] ωB97,[30] ωB97X,[30] M06,[31] and M06-2X.[31] For some functionals, we have also examined the use of dispersion corrections[32] with the Becke−Johnson damping (referred to simply as D3 in the present study).[33] The dftd3 program[32] was used to obtain these corrections.

RESULTS AND DISCUSSION

Performance for Geometry Optimization for Small Gold Clusters. We first examine the performance of the various procedures for the calculation of Au−Au distances in small gold clusters. Table 1 lists the structural parameters obtained using high-level CCSD(T)-type procedures with the various basis sets. For Au_2, it can be seen that conventional CCSD(T) gives bond lengths that are longer than the experimental value. They converge from above in the sequence 2.540 Å (def2-SVP) → 2.506 Å (def2-TZVP) → 2.496 (def2-QZVP). The CCSD(T)-F12-type methods show better agreement with experimental results.[34] In particular, the CCSD(T)-F12a procedure gives bond lengths that match experimental results remarkably well even with the modest def2-SVP and def2-TZVP basis sets. The good performance of the CCSD(T)-F12a procedure for the smaller basis sets is consistent with the general behavior of the F12a approximation.[9]

Table 1. Structural Parameters (Å) in Au_2−Au_4 Calculated Using CCSD(T)-Type Procedures

method	basis set	Au_2	Au_3	Au_4 (1)[a]	Au_4 (2)[a]
CCSD(T)	def2-SVP	2.540			
CCSD(T)	def2-TZVP	2.506			
CCSD(T)	def2-QZVP	2.496			
CCSD(T)-F12a	def2-SVP	2.479	2.532	1.289	2.304
CCSD(T)-F12a	def2-TZVP	2.476	2.519	1.288	2.298
CCSD(T)-F12a	def2-QZVP	2.479	2.522	1.294	2.308
CCSD(T)-F12b	def2-SVP	2.494	2.551	1.294	2.330
CCSD(T)-F12b	def2-TZVP	2.486	2.534	1.290	2.314
CCSD(T)-F12b	def2-QZVP	2.481	2.526	1.294	2.310
literature		2.472[b]		1.295[c]	2.310[c]

[a]Distances between the center of mass and the two distinct types of Au atoms in Au_4. [b]Ref 34. [c]Ref 3d.

For Au_3, all CCSD(T)-F12-type procedures, with all three basis sets considered, yield bond lengths that are in close agreement with one another. For Au_4 where CCSD(T)/cc-pVTZ structures have been obtained in a previous study,[3d] we find that the structural parameters obtained with CCSD(T)-F12-type methods are also in good agreement with these literature values. Overall, we consider both the CCSD(T)-F12a/def2-SVP and the CCSD(T)-F12a/def2-TZVP procedures to be reliable and cost-effective for practical applications, with the former being less demanding on computational resources and the latter being theoretically somewhat more rigorous. When it is feasible to perform calculations with the larger def2-QZVP basis set, both the CCSD(T)-F12a and CCSD(T)-F12b methods provide an accurate means for the optimization of small gold clusters.

We now use the CCSD(T)-F12b/def2-QZVP-optimized structural parameters (Table 1) for Au_2−Au_4 to evaluate the performance of a small selection of representative DFT procedures for the geometry optimization for gold clusters. The mean absolute deviations (MADs) from the benchmark values are shown in Table 2. In general, the DFT procedures perform adequately, with MADs less than 0.1 Å. Consistent with most of the CCSD(T)-type procedures, we see a systematic improvement in the performance with respect to basis set size for these DFT methods. We nonetheless deem the

Table 2. Mean Absolute Deviations (Å) from Benchmark CCSD(T)-F12b/def2-QZVP Structural Parameters for Geometries Optimized with the Various DFT Procedures

method	cc-pVDZ-PP	cc-pVTZ-PP	cc-pVQZ-PP
		pure DFT procedures	
B-LYP	0.080	0.069	0.065
B-PW91	0.048	0.036	0.032
PBE-PBE	**0.046**	**0.033**	**0.029**
M06-L	0.069	0.054	0.054
		hybrid DFT procedures	
B3-LYP	0.071	0.060	0.056
B3-PW91	0.047	0.035	0.031
PBE1-PBE	0.043	0.031	0.028
LC-ωPBE	**0.030**	**0.021**	**0.019**
B98	0.058	0.047	0.043
ωB97X	0.063	0.053	0.050
M06	0.096	0.085	0.086
M06-2X	0.090	0.075	0.071

differences in the performance for the different basis sets sufficiently small in the context of geometry optimization.

We can see that, on the whole, the hybrid DFT procedures do not uniformly outperform their pure DFT counterparts. Nonetheless, we find LC-ωPBE to be the best performing method for this set of structural parameters, with MADs that are less than 0.05 Å for all three basis sets. In addition, we can see that PBE-PBE also gives MAD values that are quite small, and it would be an attractive option in the cases where the use of hybrid DFT procedures such as LC-ωPBE becomes computationally too demanding.

Benchmark Cohesive Energies for Au_2 to Au_8. Following the identification of a suitable procedure for geometry optimization for small gold clusters, we now turn our attention to the calculation of their cohesive energies. For clusters Au_2–Au_4, we have obtained cohesive energies using the CCSD(T)-F12a procedure with the def2-TZVP and def2-QZVP basis sets. We have also obtained CCSD(T)-F12a/def2-TZVP energies for Au_5 and Au_6. In the present study, we have formulated a composite procedure for the calculation of larger gold clusters. We have applied this procedure to clusters as large as Au_8. This composite protocol is devised in the spirit of the W1X-2 procedure,[35] where a series of CCSD(T)-F12-type procedures is used to approximate the complete-basis-set (CBS) limit of frozen-core CCSD(T), and it employs MP2 for the evaluation of core–valence correlation effect.

With computational efficiency in mind, within the formulation of the composite procedure used in the present study, we do not attempt to approximate the CCSD(T)/CBS limit but rather to obtain CCSD(T) values that are sufficiently converged. We have examined the use of both the F12a-type and the F12b-type coupled-cluster procedures for the present composite procedure, and we find that the F12b-type procedures provide a slightly better performance. This is presumably due to their somewhat more systematic nature,[9] which is advantageous in the context of composite methods. Thus, the CCSD component of the CCSD(T) energy is obtained at the CCSD-F12b/def2-TZVP level, while the (T) component is obtained using the CCSD(T)-F12b/def2-SVP procedure.

For the application to gold clusters, while the 60 core electrons of a gold atom are approximated by ECPs, a total of 19 electrons ($5s^2$, $5p^6$, $5d^{10}$, $6s^1$) remain to be treated explicitly. To reduce the demand on computational resources, we include only the 5d and 6s electrons in our frozen-core (FC) CCSD(T)-F12b calculations. In accordance with W1X-2, the remaining core–valence (CV) correlation is evaluated at the MP2 level. To lessen the demand on computational resources, in the present study, we use the cc-pWCVDZ-PP basis set[12] in the MP2 calculations. The components of the resulting composite procedure are summarized in Table 3.

Table 4 shows the cohesive energies for the various gold clusters calculated with the composite method, along with those obtained with the CCSD(T)-F12a procedure. Among the three components within the composite protocol that are used to approximate full CCSD(T)-F12a calculations, namely CCSD-F12b(FC), Δ(T)-F12b(FC), and ΔCV, the CCSD-F12b(FC) component accounts for ∼86% of this part of the cohesive energy for all seven clusters considered. The two minor components Δ(T)-F12b(FC) and ΔCV each account for ∼7% of the total composite electronic energy.

We can see that, for Au_2 and Au_3, where experimental values are available,[34,36] the CCSD(T)-F12a procedure as well as the composite method give cohesive energies that are in good agreement with one another and with experimental results, when the contributions from spin–orbit effects (ΔE_{SO}) are accounted for (∼ 5 kJ mol^{-1} for Au_2 and ∼11 kJ mol^{-1} for Au_3). It is noteworthy that there is considerable variation between ΔE_{SO} values obtained using the different methods. For bulk gold, a ΔE_{SO} value of 0.141 eV (13.6 kJ mol^{-1}) has been estimated previously.[37] While this bulk ΔE_{SO} value is by no means a definitive yardstick, we deem the empirically estimated values and those given in ref 3d somewhat too large. On the other hand, the PBE-PBE-2c/dhf-TZVP-2c values obtained in the present study appear to be more consistent with this estimated bulk ΔE_{SO} value. We nonetheless caution that the ΔE_{SO} component may be a substantial contributor to the uncertainties in our calculated 0 K cohesive energies. For larger clusters (Au_4–Au_6), we also observe adequate agreement between the values obtained with the CCSD(T)-F12a procedure and those calculated by the composite protocol. Thus, it appears that the composite method provides a good approximation to the full CCSD(T)-F12a procedure.

Table 3. Components of the Composite Procedure Used for the Calculation of Cohesive Energies for Gold Clusters in the Present Study

component	method
CCSD-F12b(FC)[a]	CCSD-F12b(FC)/def2-TZVP
Δ(T)-F12b(FC)[a]	CCSD(T)-F12b(FC)/def2-SVP − CCSD-F12b(FC)/def2-SVP
ΔCV[b]	MP2(Full)/cc-pWCVDZ-PP − MP2(FC)/cc-pWCVDZ-PP

[a]FC is frozen core, where only the 5d and 6s electrons are correlated. [b]CV represents core–valence correlation, where the 5s, 5p, 5d, and 6s electrons are correlated.

Performance of DFT Procedures for the Evaluation of Cohesive Energies for Au_2–Au_8. We now apply the cohesive energies for Au_2–Au_8 calculated with the composite protocol introduced in the previous section to the benchmark of a selection of DFT procedures. As the accurate calculation of energies is often more challenging for theoretical procedures than the prediction of a reliable geometry, we have examined a larger number of DFT procedures than those found in Table 2. The mean absolute deviations (MADs) and largest deviations (LDs) for the various DFT procedures are shown in Table 5.

We first note that the results are not very sensitive to the basis set, with the use of cc-pVTZ-PP only mildly outperforming cc-pVDZ-PP. We find that the pure DFT procedures, in general, give MAD and LD values that are smaller than those for hybrid DFT methods. Interestingly, the MADs for M06-type procedures also increase with the proportion of Hartree–Fock exchange in the order M06-L (∼10 kJ mol^{-1}, 0% Hartree–Fock exchange) → M06 (∼20 kJ mol^{-1}, 27%) → M06-2X (∼60 kJ mol^{-1}, 54%). In addition, the TPSSh functional, which has the smallest proportion of Hartree–Fock exchange (10%) among the hybrid DFT procedures, gives the lowest MADs of ∼10–15 kJ mol^{-1}. For the pure DFT methods, the procedures related to the PBE exchange-correlation functional, namely PBE-PBE, PBEh-PBE, ωPBEh-PBE, TPSS-TPSS, and M06-L, yield fairly good MADs of ∼10 kJ mol^{-1}. The inclusion of dispersion corrections leads to substantially smaller MADs for many functionals. The PBE-PBE-D3 and TPSS-TPSS-D3 pure DFT procedures and the

Table 4. Cohesive Energies (0 K, kJ mol^{-1}) for Au_2−Au_8 Calculated with the Composite Method and the CCSD(T)-F12a Procedure

method	Au_2	Au_3	Au_4	Au_5	Au_6	Au_7	Au_8
			calculated scalar-relativistic energy				
composite method[a]	109.1	107.1	150.0	167.1	193.0	191.6	202.4
CCSD-F12b(FC)	95.6	91.4	128.6	144.1	167.6	165.5	175.4
Δ(T)-F12b(FC)	6.8	7.7	11.0	11.4	12.0	12.5	12.4
ΔCV	7.2	8.6	11.3	12.7	14.6	14.8	15.8
ΔZPVE	−0.6	−0.6	−1.0	−1.1	−1.2	−1.2	−1.2
CCSD(T)(Full)-F12a/def2-TZVP	109.4	108.0	151.5	169.9	193.2		
CCSD(T)(Full)-F12a/def2-QZVP	109.3	107.6	148.8				
			contribution from spin−orbit effects (ΔE_{SO})				
PBE-PBE-2c/def2-QZVPP[b]	3.2	10.5					
TPSS-TPSS-2c/aug-cc-pVTZ[c]	6.3	13.1	14.6				
PBE-PBE-2c/def2-TZVP-2c[d]	4.5	8.8	12.5	12.6	11.5	12.6	11.7
estimated[e]	7.8	12.5	14.9	16.3	17.3	17.9	17.3
			experimental cohesive energy[f]				
	112.1	122.2					

[a]See Table 3 for the definition of the components of the composite method. [b]Ref 3e. [c]Ref 3d by a two-component treatment that is different from the one used in the present study. [d]This work. [e]Estimated with the empirical formula in ref 3d. [f]Refs 34 and 36.

Table 5. Statistical Performance (kJ mol^{-1}) Against Benchmark Cohesive Energies (Composite CCSD(T)-F12b) for Au_2−Au_8 for the Various DFT Procedures

	cc-pVDZ-PP		cc-pVTZ-PP		cc-pVTZ + D3	
method	MAD[a]	LD[b]	MAD[a]	LD[b]	MAD[a]	LD[b]
			pure DFT procedures			
B-LYP	29.8	−42.9	27.1	−39.6	12.9	−19.0
B-PW91	19.4	−28.7	16.4	−25.1		
PBE-PBE	10.9	−17.3	8.9	−13.7	4.6	9.8
PBEh-PBE	10.3	−16.3	8.4	−12.7	5.8	14.3
ωPBEh-PBE	10.3	−16.3	8.4	−12.7		
TPSS-TPSS	9.1	−14.5	6.9	−10.7	3.2	10.8
M06-L	10.3	−16.6	7.7	−12.4	7.6	−12.2
			hybrid DFT procedures			
B3-LYP	36.7	−49.6	34.0	−46.2	32.0	36.9
B3-PW91	29.2	−39.2	26.3	−35.7	13.3	−17.9
CAM-B3-LYP	35.7	−46.5	33.2	−43.3	25.6	−32.8
PBE1-PBE	25.1	−33.8	22.2	−30.3	16.1	−21.9
PBEh1-PBE	24.4	−33.1	21.5	−29.5	9.7	−13.5
LC-ωPBE	34.8	−42.1	32.4	−39.1	24.5	−28.1
HSEh1-PBE	23.5	−32.1	20.5	−28.4		
TPSSh	14.8	−22.0	11.8	−18.2	3.3	5.0
B1-B95	25.1	−33.5	22.4	−30.2	3.3	−5.1
B98	26.2	−37.6	23.6	−34.3	12.5	−19.1
ωB97	21.0	−29.4	17.8	−25.7		
ωB97X	25.8	−35.5	22.8	−31.9		
M06	22.3	−32.0	19.5	−28.7	19.0	−27.9
M06-2X	60.4	−74.2	57.0	−70.3	56.9	−70.1

[a]MAD is mean absolute deviation. [b]LD is largest deviation.

hybrid DFT methods TPSSh-D3 and B1-B95-D3 are among the best performers.

Cohesive Energies for Larger Gold Clusters. We now briefly recapitulate the major results of the present study so far. We have devised a composite protocol that is accurate for the calculation of cohesive energies of gold clusters and has a moderate demand on computational resources. Using benchmark structures and cohesive energies obtained with high-level CCSD(T)-F12-type procedures and the composite procedure, we find that the PBE-PBE and LC-ωPBE DFT methods give adequate geometries for small gold clusters, and that PBE-PBE-D3 and TPSS-TPSS-D3 yield cohesive energies that are quite accurate.

We now apply this knowledge to the calculation of cohesive energies for larger gold clusters, and we base our protocol on the PBE-PBE functional as it gives adequate descriptions for both geometries (Table 2) as well as energies (Table 5). Thus, we optimize the geometries at the PBE-PBE/cc-pVDZ-PP level and obtain ZPVEs using the corresponding unscaled harmonic frequencies. The energies are then calculated with (1) the PBE-PBE/cc-pVTZ-PP procedure, (2) its dispersion corrected variant, and, finally, (3) the total energy with the inclusion of ΔE_{SO} obtained from PBE-PBE-2c/dhf-TZVP-2c calculations. The PBE-PBE, PBE-PBE-D3, and the ΔE_{SO}-inclusive PBE-PBE-D3 cohesive energies for Au_2−Au_{20} are shown in Table 6, together with the corresponding values for Au_2−Au_8 obtained with the composite method.

To further elucidate the performance of this proposed protocol, we note that these calculated cohesive energies for Au_2−Au_{20} could be used to obtain the bulk cohesive energy for solid gold using the empirical correlation $E \propto n^{-1/3}$, where n is the number of gold atoms in the cluster.[38] A plot of the cohesive energies versus the $n^{-1/3}$ values is shown in Figure 1. We first note that the linear fits are quite good, with R^2 values that are larger than 0.98 for all three lines. The bulk cohesive energies estimated by PBE-PBE, PBE-PBE-D3, and PBE-PBE-D3 + ΔE_{SO} are 328.5, 359.9, and 383.2 kJ mol^{-1}, respectively, which compare reasonably well with the experimental value of 368 kJ mol^{-1}.[39] It is noteworthy that the PBE-PBE-D3 and PBE-PBE-D3 + ΔE_{SO} values suggest a ΔE_{SO} of 23.3 kJ mol^{-1}, which is somewhat larger than the calculated value given in ref 37 (13.6 kJ mol^{-1}). Using this alternative value for ΔE_{SO} leads to an estimated bulk cohesive energy of 373.5 kJ mol^{-1}, which is in better agreement with the experimental value.

The calculation of atomization energies is a challenging problem for computational chemistry methods, and the present study provides a starting point toward accurate modeling of the chemistry of gold clusters. However, we emphasize that the results and recommendations are based on the observations made on one (challenging) thermochemical property. We thus

Table 6. Calculated Cohesive Energies (0 K, kJ mol^{-1}) for Au_2−Au_{20}[a]

	composite method[b]	PBE-PBE[b]	PBE-PBE-D3[b]	PBE-PBE-D3 + ΔE_{SO}[c]
Au_2	109.1	110.3	112.2	116.7
Au_3	107.1	114.5	117.8	126.6
Au_4	150.0	145.5	150.8	163.3
Au_5	167.1	159.3	165.7	178.3
Au_6	193.0	181.9	189.2	200.7
Au_7	191.6	177.9	185.9	198.4
Au_8	202.4	189.2	197.6	209.3
Au_9		191.1	200.4	213.7
Au_{10}		199.0	209.0	222.2
Au_{11}		199.3	210.2	223.6
Au_{12}		205.8	216.7	231.2
Au_{13}		204.8	215.8	230.3
Au_{14}		209.3	225.0	240.3
Au_{15}		209.2	225.9	238.5
Au_{16}		212.7	229.6	245.2
Au_{17}		215.7	233.2	249.6
Au_{18}		219.3	237.2	253.1
Au_{19}		220.8	238.9	252.2
Au_{20}		225.3	243.4	258.7

[a]The cc-pVTZ-PP basis set is used for the DFT calculations. [b]The ΔE_{SO} components are not included. [c]Obtained from PBE-PBE-2c/dhf-TZVP-2c calculations.

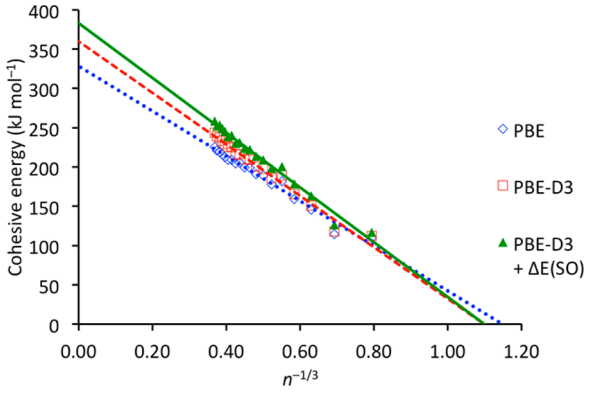

Figure 1. Calculated cohesive energies versus $n^{-1/3}$ for Au_n with n = 2−20.

note that further generalization to other properties of gold clusters would be premature at this stage.

CONCLUDING REMARKS

High-level CCSD(T)-F12-type procedures have been used to assess the performance of a variety of computationally less demanding methods for the calculation of cohesive energies for small to medium-sized gold clusters. For geometry optimization for small gold clusters, the CCSD(T)-F12a procedure is found to be quite effective when combined with a triple-ζ (def2-TZVP) or even just a double-ζ (def2-SVP) basis set, when compared with the benchmark geometries. We find that two DFT procedures, namely LC-ωPBE and PBE-PBE, give structures that are in close agreement with the benchmark.

For the calculation of single-point energies, we have devised a composite protocol and show that it provides a good approximation to those obtained from direct CCSD(T)-F12a calculations using the def2-TZVP or def2-QZVP basis sets. We have obtained benchmark cohesive energies for Au_2−Au_8 using this composite procedure and assessed a number of DFT methods for the calculation of the cohesive energies. The PBE-PBE-D3 and TPSS-TPSS-D3 pure DFT procedures and the hybrid DFT methods TPSSh-D3 and B1-B95-D3 are shown to give adequate values against the benchmark. The contributions from spin−orbit effects have been obtained from a number of sources but show considerable variations in the results. We nonetheless deem PBE-PBE-2c/dhf-TZVP-2c used in the present study a reasonable method for the calculation of spin−orbit contributions to cohesive energies for small to medium-sized gold clusters.

In closing, we give a brief summary for the definition of the composite protocol and our recommended DFT procedure for the calculation of cohesive energies of gold clusters. Thus, in both cases, geometries and unscaled zero-point vibrational energies are obtained at the PBE-PBE/cc-pVDZ-PP level.

The composite protocol contains the following components: a base energy obtained at the CCSD-F12b(FC)/def2-TZVP level where FC indicates that only the 5d and 6s electrons are correlated; a correction term for perturbative triples [Δ(T)-F12b(FC)] obtained by CCSD(T)-F12b(FC)/def2-SVP − CCSD-F12b(FC)/def2-SVP; and a correction for core−valence correlations [ΔCV] obtained by MP2(Full)/cc-pWCVDZ-PP − MP2(FC)/cc-pWCVDZ-PP, where Full indicates that the 5s, 5p, 5d, and 6s electrons are correlated.

For DFT, we recommend the use of PBE-PBE-D3/cc-pVTZ-PP for its good agreement with the composite procedure as well as its computational efficiency.

Finally, in both cases, a ΔE_{SO} term is incorporated using a two-component calculation at the PBE-PBE-2c/dhf-TZVP-2c level.

ASSOCIATED CONTENT

Supporting Information

PBE-PBE/cc-pVDZ-PP geometries in xyz format incorporated in a single zip file (au_clusters_geom.zip), key Au−Au distances for Au_2−Au_4 (Table S1); calculated electronic energies for Au_2−Au_8 at the various levels of theory (Table S2); and PBE-PBE/cc-pVDZ-PP zero-point vibrational energies, PBE-PBE-2c/dhf-TZVP-2c spin−orbit corrections, dispersion corrections, PBE-PBE/cc-pVTZ-PP electronic energies, and calculated 0 K cohesive energies for all species (Table S3). This material is available free of charge via the Internet at http://pubs.acs.org.

AUTHOR INFORMATION

Corresponding Author

*E-mail: chan_b@chem.usyd.edu.au (B.C.); yimwl@ihpc.a-star.edu.sg (W.-L.Y.).

Notes

The authors declare no competing financial interest.

ACKNOWLEDGMENTS

We gratefully acknowledge funding from the Australian Research Council (to B.C.) and Institute of High Performance Computing (to W.-L.Y. for an IHPC Independent Investigatorship) and generous grants of computer time (to B.C.) from the National Computational Infrastructure (NCI) National Facility and Intersect Australia Ltd.

REFERENCES

(1) For extensive reviews, see for example: (a) Daniel, M.-C.; Astruc, D. *Chem. Rev.* **2004**, *104*, 293−346. (b) Sperling, R. A.; Rivera Gil, P.; Zhang, F.; Zanella, M.; Parak, W. J. *Chem. Soc. Rev.* **2008**, *37*, 1896−1908.

(2) For recent reviews, see for example: (a) Chen, Y.; Crawford, P.; Hu, P. *Catal. Lett.* **2007**, *119*, 21−28. (b) Chretien, S.; Buratto, S. K.; Metiu, H. *Curr. Opin. Solid State Mater. Sci.* **2008**, *11*, 62−75. (c) Tian, D.; Zhao, J. *J. Comput. Theor. Nanosci.* **2009**, *6*, 318−326. (d) Johnson, G. E.; Mitric, R.; Bonacic-Koutecky, V.; Castleman, A. W. *Chem. Phys. Lett.* **2009**, *475*, 1−9. (e) Schwerdtfeger, P.; Lein, M. *Gold Chem.* **2009**, 183−247. See also: (f) Yim, W.-L.; Nowitzki, T.; Necke, M.; Schnars, H.; Nickhut, P.; Biener, J.; Biener, M.; Zielasek, V.; Al-Shamery, K.; Klüner, T.; Bäumer, M. *J. Phys. Chem. C* **2007**, *111*, 445−451.

(3) For recent studies, see for example: (a) Olson, R. M.; Varganov, S.; Gordon, M. S.; Metiu, H.; Chretien, S.; Piecuch, P.; Kowalski, K.; Kucharski, S. A.; Musial, M. *J. Am. Chem. Soc.* **2005**, *127*, 1049−1052. (b) Diefenbach, M.; Kim, K. S. *J. Phys. Chem. B* **2006**, *110*, 21639−21642. (c) Choi, Y. C.; Kim, W. Y.; Lee, H. M.; Kim, K. S. *J. Chem. Theory Comput.* **2009**, *5*, 1216−1223. (d) Shi, Y.-K.; Li, H. Z.; Fan, K.-N. *J. Phys. Chem. A* **2010**, *114*, 10297−10308. (e) Fabiano, E.; Constantin, L. A.; Sala, F. D. *J. Chem. Phys.* **2011**, *134*, 194112−1−10. (f) Lee, H. M.; Kim, K. S. *Chem.—Eur. J.* **2012**, *18*, 13203−13207.

(4) See for example: (a) Hehre, W. J.; Radom, L.; Schleyer, P. v. R.; Pople, J. A. *Ab Initio Molecular Orbital Theory*; Wiley: New York, 1986. (b) Jensen, F. *Introduction to Computational Chemistry*, 2nd ed.; Wiley: Chichester, U. K., 2007. (c) Koch, W.; Holthausen, M. C. *A Chemist's Guide to Density Functional Theory*, 2nd ed.; Wiley: New York, 2001.

(5) Frisch, M. J.; Trucks, G. W.; Schlegel, H. B.; Scuseria, G. E.; Robb, M. A.; Cheeseman, J. R.; Scalmani, G.; Barone, V.; Mennucci, B.; Petersson, G. A.; Nakatsuji, H.; Caricato, M.; Li, X.; Hratchian, H. P.; Izmaylov, A. F.; Bloino, J.; Zheng, G.; Sonnenberg, J. L.; Hada, M.; Ehara, M.; Toyota, K.; Fukuda, R.; Hasegawa, J.; Ishida, M.; Nakajima, T.; Honda, Y.; Kitao, O.; Nakai, H.; Vreven, T.; Montgomery, J. A., Jr.; Peralta, J. E.; Ogliaro, F.; Bearpark, M.; Heyd, J. J.; Brothers, E.; Kudin, K. N.; Staroverov, V. N.; Kobayashi, R.; Normand, J.; Raghavachari, K.; Rendell, A.; Burant, J. C.; Iyengar, S. S.; Tomasi, J.; Cossi, M.; Rega, N.; Millam, N. J.; Klene, M.; Knox, J. E.; Cross, J. B.; Bakken, V.; Adamo, C.; Jaramillo, J.; Gomperts, R.; Stratmann, R. E.; Yazyev, O.; Austin, A. J.; Cammi, R.; Pomelli, C.; Ochterski, J. W.; Martin, R. L.; Morokuma, K.; Zakrzewski, V. G.; Voth, G. A.; Salvador, P.; Dannenberg, J. J.; Dapprich, S.; Daniels, A. D.; Farkas, Ö.; Foresman, J. B.; Ortiz, J. V.; Cioslowski, J.; Fox, D. J. *Gaussian 09*, revision A.02; Gaussian, Inc.: Wallingford, CT, 2009.

(6) Werner, H.-J.; Knowles, P. J.; Manby, F. R.; Schütz, M.; Celani, P.; Knizia, G.; Korona, T.; Lindh, R.; Mitrushenkov, A.; Rauhut, G.; Adler, T. B.; Amos, R. D.; Bernhardsson, A.; Berning, A.; Cooper, D. L.; Deegan, M. J. O.; Dobbyn, A. J.; Eckert, F.; Goll, E.; Hampel, C.; Hesselmann, A.; Hetzer, G.; Hrenar, T.; Jansen, G.; Köppl, C.; Liu, Y.; Lloyd, A. W.; Mata, R. A.; May, A. J.; McNicholas, S. J.; Meyer, W.; Mura, M. E.; Nicklaß, A.; Palmieri, P.; Pflüger, K.; Pitzer, R.; Reiher, M.; Shiozaki, T.; Stoll, H. Stone, A. J.; Tarroni, R.; Thorsteinsson, T.; Wang, M.; Wolf, A. *MOLPRO 2010.1*; University College Cardiff Consultants Limited: Cardiff, U. K., 2010.

(7) Ahlrichs, R.; Bär, M. Häser, M.; Horn, H.; Kölmel, C. *Chem. Phys. Lett.* **1989**, *162*, 165−169. See also: www.turbomole.com.

(8) Assadollahzadeh, B.; Schwerdtfeger, P. *J. Chem. Phys.* **2009**, *131*, 064306−1−11.

(9) (a) Adler, T. B.; Knizia, G.; Werner, H.-J. *J. Chem. Phys.* **2007**, *127*, 221106−1−4. (b) Knizia, G.; Adler, T. B.; Werner, H.-J. *J. Chem. Phys.* **2009**, *130*, 054104−1−20.

(10) For recent reviews on explicitly correlated methods such as F12, see for example: (a) Klopper, W.; Manby, F. R.; Ten-No, S.; Valeev, E. F. *Int. Rev. Phys. Chem.* **2006**, *25*, 427−468. (b) Shiozaki, T.; Valeev, E. F.; Hirata, S. *Ann. Rep. Comput. Chem.* **2009**, *5*, 131−148. (c) Werner, H.-J.; Knizia, G.; Adler, T. B.; Marchetti, O. *Z. Phys. Chem.* **2010**, *224*, 493−511. (d) Kong, L.; Bischoff, F. A.; Valeev, E. F. *Chem. Rev.* **2012**, *112*, 75−107. (e) Hättig, C.; Klopper, W.; Köhn, A.; Tew, D. P. *Chem. Rev.* **2012**, *112*, 4−74.

(11) Weigend, F.; Ahlrichs, R. *Phys. Chem. Chem. Phys.* **2005**, *7*, 3297−3305.

(12) Peterson, K. A.; Puzzarini, C. *Theor. Chem. Acc.* **2005**, *114*, 283−296.

(13) As the use of ECPs excludes correlation effects for inner-shell electrons, which may have notable contributions to the cohesive energy, we have therefore briefly examined this aspect. At the MP2/UGBS level, we have obtained the cohesive energies for Au_2 and Au_3 using two options for the frozen-core treatment. In one type of frozen-core treatment, the 1s−4f orbitals are frozen, which is consistent with the rest of the correlation calculations in the present study. In another treatment, the core size is reduced substantially to that for Ar, i.e., 1s−3p. We find that the use of the smaller core leads to an increase in the cohesive energies by 0.9 and 1.0 kJ mol^{-1} for Au_2 and Au_3, respectively. A survey of the data used in ref 35 also shows that, on a per atom basis, the contributions of inner-shell correlations to the atomization energies are typically ∼0.5−1.5 kJ mol^{-1} for a set of 148 molecules. Thus, we deem further inclusion of inner-shell correlation effects in the present study not cost-effective with respect to the target accuracy.

(14) Armbruster, M. K.; Weigend, F.; van Wüllen, C.; Klopper, W. *Phys. Chem. Chem. Phys.* **2008**, *10*, 1748−1756.

(15) Perdew, J. P.; Burke, K.; Ernzerhof, M. *Phys. Rev. Lett.* **1996**, *77*, 3865−3868.

(16) Weigend, F.; Baldes, A. *J. Chem. Phys.* **2010**, *133*, 174102.

(17) Johnson, B. G.; Gill, P. M. W.; Pople, J. A. *J. Chem. Phys.* **1993**, *98*, 5612−5626.

(18) (a) Becke, A. D. *Phys. Rev. A* **1988**, *38*, 3098−3100. (b) Perdew, J. P. In *Electronic Structure of Solids '91*; Ziesche, P., Eschrig, H., Eds.; Akademie Verlag: Berlin, 1991; p 11.

(19) Ernzerhof, M.; Perdew, J. P. *J. Chem. Phys.* **1998**, *109*, 3313−3320.

(20) Heyd, J.; Scuseria, G. E.; Ernzerhof, M. *J. Chem. Phys.* **2006**, *124*, 219906−1−1.

(21) Tao, J. M.; Perdew, J. P.; Staroverov, V. N.; Scuseria, G. E. *Phys. Rev. Lett.* **2003**, *91*, 146401−1−4.

(22) Zhao, Y.; Truhlar, D. G. *J. Chem. Phys.* **2006**, *125*, 194101−1−18.

(23) Stephens, P. J.; Devlin, F. J.; Chabalowski, C. F.; Frisch, M. J. *J. Phys. Chem.* **1994**, *98*, 11623−11627.

(24) Becke, A. D. *J. Chem. Phys.* **1993**, *98*, 1372−1377.

(25) Yanai, T.; Tew, D.; Handy, N. *Chem. Phys. Lett.* **2004**, *393*, 51−57.

(26) Adamo, C.; Barone, V. *J. Chem. Phys.* **1999**, *110*, 6158−6170.

(27) Vydrov, O. A.; Scuseria, G. E. *J. Chem. Phys.* **2006**, *125*, 234109-1−9.

(28) Becke, A. D. *J. Chem. Phys.* **1996**, *104*, 1040−1046.

(29) Schmider, H. L.; Becke, A. D. *J. Chem. Phys.* **1998**, *108*, 9624−9631.

(30) Chai, J.-D.; Head-Gordon, M. *J. Chem. Phys.* **2008**, *128*, 084106−1−15.

(31) Zhao, Y.; Truhlar, D. G. *Theor. Chem. Acc.* **2008**, *120*, 215−241.

(32) Grimme, S.; Antony, J.; Ehrlich, S.; Krieg, H. *J. Chem. Phys.* **2010**, *132*, 154104-1−19.

(33) (a) Becke, A. D.; Johnson, E. *J. Chem. Phys.* **2005**, *122*, 154101-1−11. (b) Grimme, S.; Ehrlich, S.; Goerigk, L. *J. Comput. Chem.* **2011**, *32*, 1456−1465 and references therein.

(34) (a) Bishea, G. A.; Morse, M. D. *J. Chem. Phys.* **1991**, *95*, 5646−5659. (b) James, A. M.; Kowalczyk, P.; Simard, B.; Pinegar, J. C.; Morse, M. D. *J. Mol. Spectrosc.* **1994**, *168*, 248−257.

(35) Chan, B.; Radom, L. *J. Chem. Theory Comput.* **2012**, *8*, 4259−4269.

(36) Hilpert, K.; Gingerich, K. A. *Ber. Bunsen-Ges. Phys. Chem.* **1980**, *84*, 739−745.

(37) Yang, Z.; Zhou, H.; Weng, H.; Dong, J. *Appl. Phys. Lett.* **2008**, *92*, 023115−1−3.

(38) See ref 8 for the use of such an extrapolation scheme using Au_2−Au_{20} with a different set of DFT procedures. We note that, in principle, such a correlation is best applied to gold clusters of the same symmetry and spin (i.e., singlet for Au_2, Au_4, etc. and doublet for Au_3, Au_5, etc.). Nonetheless, it is apparent from Figure 1 that the correlation is already quite good for all clusters examined in the present study. We therefore include all the clusters in the extrapolations.

(39) Kittel. C. *Introduction to Solid State Physics*, 8th ed.; John Wiley & Sons: Hoboken, NJ, 2005; p 50.